

Proximity-induced negative magnetoresistance and anomalous Hall effect in monolayer graphene/CrSBr heterojunctions

Bin Dai(戴彬), Ke Zhu(祝轲), Chenyu Bai(白晨宇), Yechao Han(韩烨超), Guojing Hu(胡国静), Ruwen Wang(王汝文), Senhao Lv(吕森浩), Haisen Liu(刘海森), Zhen Zhao(赵振), Jianchen Lu(卢建臣), Hui Guo(郭辉), Haitao Yang(杨海涛), and Hong-Jun Gao(高鸿钧)

Citation: Chin. Phys. B, 2026, 35 (**7**): 077201. DOI: 10.1088/1674-1056/ae64d4
http://cpb.iphy.ac.cn; http://iopscience.iop.org/cpb

What follows is a list of articles you may be interested in

Large anomalous Hall and Nernst effect in the breathing kagome ferromagnet $NdCrGe_3$

Yang Liu(刘洋), Meng Lyu(吕孟), Junyan Liu(刘俊艳), Yibo Wang(王一博), Jinying Yang(杨金颖), Binbin Wang(王彬彬), Xiyang Li(李西阳), and Enke Liu(刘恩克)

Chin. Phys. B, 2026, 35 (**5**): 057201. DOI: 10.1088/1674-1056/ae44f0

Anomalous Hall effect in Bernal tetralayer graphene enhanced by spin-orbit interaction

Zhuangzhuang Qu(曲壮壮), Zhihao Chen(陈志豪), Xiangyan Han(韩香岩), Zhiyu Wang(王知雨), Zhuoxian Li(李卓贤), Qianling Liu(刘倩伶), Wenjun Zhao(赵文俊), Kenji Watanabe, Takashi Taniguchi, Zhi-Gang Cheng(程智刚), Zizhao Gan(甘子钊), and Jianming Lu(路建明)

Chin. Phys. B, 2025, 34 (**3**): 037201. DOI: 10.1088/1674-1056/adb411

Current-perpendicular-to-plane transport properties of 2D ferromagnetic material $CrTe_2$

Jin Wang(王瑾), Yu Liu(刘宇), Taikun Wang(王太坤), Yongkang Xu(徐永康), Shuanghai Wang(王双海), Kun He(何坤), Yafeng Deng(邓亚峰), Pengfei Yan(闫鹏飞), and Liang He(何亮)

Chin. Phys. B, 2024, 33 (**9**): 097201. DOI: 10.1088/1674-1056/ad5af1

The origin of spin current in YIG/nonmagnetic metal multilayers at ferromagnetic resonance

Yun Kang(康韵), Hai Zhong(钟海), Runrun Hao(郝润润), Shujun Hu(胡树军), Shishou Kang(康仕寿), Guolei Liu(刘国磊), Yin Zhang(张引), Xiangrong Wang(王向荣), Shishen Yan(颜世申), Yong Wu(吴勇), Shuyun Yu(于淑云), Guangbing Han(韩广兵), Yong Jiang(姜勇), Liangmo Mei(梅良模)

Chin. Phys. B, 2017, 26 (**4**): 047202. DOI: 10.1088/1674-1056/26/4/047202

Recent observations of negative longitudinal magnetoresistance in semimetal

Xi-Tong Xu(许锡童), Shuang Jia(贾爽)

Chin. Phys. B, 2016, 25 (**11**): 117204. DOI: 10.1088/1674-1056/25/11/117204

RAPID COMMUNICATION

Proximity-induced negative magnetoresistance and anomalous Hall effect in monolayer graphene/CrSBr heterojunctions

Bin Dai(戴彬)[1,2,†], Ke Zhu(祝轲)[2,†], Chenyu Bai(白晨宇)[2,3,†], Yechao Han(韩烨超)[3], Guojing Hu(胡国静)[3], Ruwen Wang(王汝文)[2,3], Senhao Lv(吕森浩)[2], Haisen Liu(刘海森)[1,2], Zhen Zhao(赵振)[2], Jianchen Lu(卢建臣)[1,‡], Hui Guo(郭辉)[2,3,§], Haitao Yang(杨海涛)[2,3], and Hong-Jun Gao(高鸿钧)[2,3]

[1] *Faculty of Materials Science and Engineering, Kunming University of Science and Technology, Kunming* 650093, *China*
[2] *Beijing National Center for Condensed Matter Physics and Institute of Physics, Chinese Academy of Sciences, Beijing* 100190, *China*
[3] *School of Physical Sciences, University of Chinese Academy of Sciences, Beijing* 100049, *China*

(Received 12 March 2026; revised manuscript received 21 April 2026; accepted manuscript online 27 April 2026)

The integration of graphene with magnetic insulators to invoke the magnetic proximity effect provides a powerful route toward spintronic devices that preserve graphene's exceptional transport characteristics. A persistent challenge, however, is the identification of magnetic substrates that are both air-stable and capable of forming high-quality van der Waals interfaces. Here, we present a magnetotransport investigation of monolayer graphene coupled to a layered A-type antiferromagnetic semiconductor CrSBr nanoflake, which is notable for its high Néel temperature ($\sim$ 132 K) and outstanding environmental stability. High-quality heterojunctions are obtained via a dry-transfer technique to ensure an atomically clean interface. Pronounced negative magnetoresistance and anomalous Hall effect in graphene are observed, arising from the suppression of spin-disorder scattering induced by the proximity exchange field from the CrSBr layer. Moreover, the heterojunction exhibits clear two-frequency Shubnikov–de Haas oscillations, evidencing the emergence of Fermi surface reconstruction in the monolayer graphene. Our results demonstrate that antiferromagnetic CrSBr can impose a robust magnetic proximity effect that manipulates the spin degrees of freedom in graphene, opening new opportunities for spintronic functionalities in two-dimensional materials.

Keywords: magnetic proximity effect, negative magnetoresistance, anomalous Hall effect, Shubnikov–de Haas oscillation

PACS: 72.80.Vp, 73.43.Qt, 85.75.–d

DOI: 10.1088/1674-1056/ae64d4 **CSTR:** 32038.14.CPB.ae64d4

1. Introduction

Two-dimensional (2D) materials continue to reshape the landscape of spin-based electronics. Graphene, with its exceptionally high carrier mobility ($> 10^5$ cm$^2\cdot$V$^{-1}\cdot$s^{-1}) and long spin diffusion length ($\sim$ 30 μm) that persist up to room temperature, provides an ideal platform for low-dissipation spin transport.[1,2] However, the absence of intrinsic magnetic order in pristine graphene limits its direct applications in spintronic devices. A widely adopted strategy to overcome this limitation is the magnetic proximity effect (MPE), whereby an exchange field is induced in graphene through intimate contact with a magnetic insulator.[3–9] The resulting exchange splitting can break time-reversal symmetry and generate spin-polarized carriers in the graphene.[10]

Compared to ferromagnetic materials, antiferromagnetic materials possess a net zero magnetic moment, thereby avoiding stray fields that could degrade device performance while offering strong stability against external magnetic perturbations.[11–16] Theoretical models predict that exchange interactions at the graphene/antiferromagnet interface can break time-reversal symmetry and induce an effective exchange field, leading to spin band splitting in graphene.[17] Among the van-der-Waals (vdW) magnets, the layered A-type antiferromagnet CrSBr stands out because of its relatively high Néel temperature ($T_N \sim 132$ K) and robust environmental stability, whereas other 2D magnets such as CrI_3 are known to be unstable under ambient conditions.[18–21] Recent studies have demonstrated that monolayer CrSBr can impose a sizable exchange field on an adjacent graphene layer, manifested as a gate-tunable spin polarization and a measurable exchange shift of 27–32 meV in the graphene band structure.[22] However, comprehensive transport signatures, particularly quantum effects under high magnetic fields, that directly link the proximity-induced exchange to modifications of the Fermi surface remain scarce.

In this work, we report the magnetotransport properties of a high-quality monolayer graphene/CrSBr heterojunction. Our measurements reveal a clear MPE in monolayer graphene induced by a CrSBr nanoflake, giving rise to a pronounced negative magnetoresistance (NMR) of up to −23%. Furthermore,

[†]These authors contributed equally to this work.
[‡]Corresponding author. E-mail: jclu@kust.edu.cn
[§]Corresponding author. E-mail: guohui@iphy.ac.cn

© 2026 Chinese Physical Society and IOP Publishing Ltd. All rights, including for text and data mining, AI training, and similar technologies, are reserved.

the presence of an exchange field modifies the well-established Dirac spectrum of graphene, resulting in unusual electronic transport behavior in the quantum oscillation regime. Two-frequency Shubnikov–de Haas (SdH) oscillations are observed in the heterojunction at low temperatures. In addition, the transverse Hall resistance exhibits a pronounced deviation from the linear dependence expected for a single-carrier Dirac system, evidencing the existence of an anomalous Hall effect (AHE). Our results confirm the capability of antiferromagnetic CrSBr to engineer spin-selective electronic structures in graphene, paving the way for developing high-performance, multifunctional spintronic architectures.

2. Experiment details

The high-quality CrSBr single crystals were synthesized through a chemical vapor transport (CVT) method.[23,24] High-purity Cr powder (99.95%), $CrBr_3$ powder (99%), and S powder (99.9995%) were thoroughly mixed and sealed in a quartz ampoule under high-vacuum conditions. The ampoule was placed in a two-zone horizontal furnace, with the hot zone and the cold zone maintained at 950 °C and 850 °C, respectively, for 72 hours. Finally, the CrSBr single crystals were obtained after the furnace was cooled naturally to room temperature.

Large-area monolayer graphene and CrSBr nanoflakes were exfoliated onto a SiO_2/Si substrate that was pretreated with oxygen plasma. Subsequently, a polymer stack was employed to selectively transfer the exfoliated flakes. The monolayer graphene was picked up using a h-BN nanoflake and then precisely released onto the pre-exfoliated CrSBr nanoflake.[25] The polymer residue was removed by immersing the stacked heterojunction in acetone.

The Hall bar devices of the heterojunction were fabricated using standard e-beam lithography (Raith 150), followed by deposition of Cr/Au electrodes (5 nm/35 nm). Prior to metal deposition, the top h-BN layer was selectively removed by SF_6 reactive ion etching (RIE) to expose the graphene contact regions. The thicknesses of the heterojunctions were determined using a commercial atomic force microscope (AFM, Oxford Instruments Cypher S). Raman spectra were acquired using a WITec ALPHA300R system. Electrical transport measurements were conducted using a standard four-terminal configuration within a physical property measurement system (PPMS, Dyna-Cool, Quantum Design).

3. Results and discussion

Figure 1(a) illustrates the crystal structures of monolayer graphene and a CrSBr nanoflake, where vdW interactions are formed between the two layers after the heterostructure is assembled using a dry-transfer technique. The device configuration discussed in this work is shown in Fig. 1(b). Figure 1(c) presents the Raman spectra of the monolayer graphene, h-BN, CrSBr, and the heterojunction, all measured on a SiO_2/Si substrate. The characteristic Raman peaks of both CrSBr and monolayer graphene are clearly preserved in the spectrum of the heterojunction, indicating the formation of a high-quality vdW interface between the two layers. Figure 1(d) shows the AFM image of the device and the corresponding height profile extracted along the white line, showing a thickness of ∼ 3.2 nm for the CrSBr nanoflake.

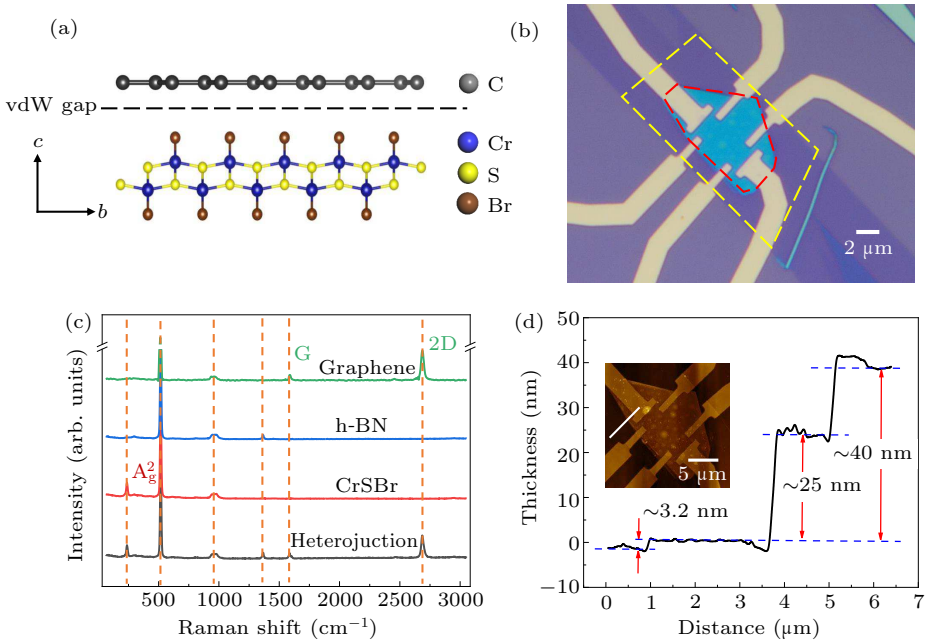


Fig. 1. Structural characterizations of a graphene/CrSBr heterojunction. (a) Schematic illustration of the crystal structure of the graphene/CrSBr heterojunction. (b) Optical micrograph of the fabricated device consisting of an h-BN/graphene/CrSBr heterojunction on a SiO_2/Si substrate with Cr–Au electrodes. The red dash line outlines the h-BN/graphene regions, while the yellow dash line indicates the underlying CrSBr layer. (c) Raman spectra of 1L graphene, h-BN, CrSBr and heterojunction on a SiO_2/Si substrate. (d) The height profile along the white line of the AFM image (inset), showing thicknesses of the CrSBr nanoflake (∼ 3.2 nm), the h-BN/graphene (∼ 25 nm), and the Cr–Au electrode (∼ 40 nm).

The magnetic properties of the synthesized CrSBr bulk crystal were first characterized. Temperature-dependent magnetic susceptibility measurements under zero-field-cooled (ZFC) and field-cooled (FC) procedures reveal a sharp cusp at $T_N = 132$ K (Fig. 2(a)), consistent with previous reports and signaling the onset of antiferromagnetic order.[18] A weak ferromagnetic-like feature emerges below 27.5 K, which may arise from defects in the crystals.[26,27] Figure 2(b) displays the field-dependent magnetization with the external field applied along the crystallographic c axis. Below T_N, the magnetic state of CrSBr undergoes a transition from canted antiferromagnetism to field-polarized ferromagnetism as the external field increases beyond the saturation field B_{sat}, which has been reported to be comparable in the bulk and few-layer CrSBr.[27,28]

Figure 2(c) presents the longitudinal magnetoresistance ratio (MRR $= R(B)/R(0)$) measured under an out-of-plane magnetic field. Across the entire temperature range, the heterojunction exhibits clear NMR. At 180 K, which is above T_N, the sample exhibits a broad NMR response, whereas below T_N, the NMR shows a distinct two-regime behavior. Taking the curve measured at 2 K as an example, the MR drops steeply as the magnetic field increases up to about 2.1 T and then gradually saturates at higher fields. The characteristic transition field B_{trans} (~ 2.1 T) is marked by the dashed line in Fig. 2(c). Such two-regime behavior, an initial rapid drop followed by a plateau, suggests a strong coupling between the magnetic order of CrSBr and the charge carriers in the adjacent monolayer graphene.

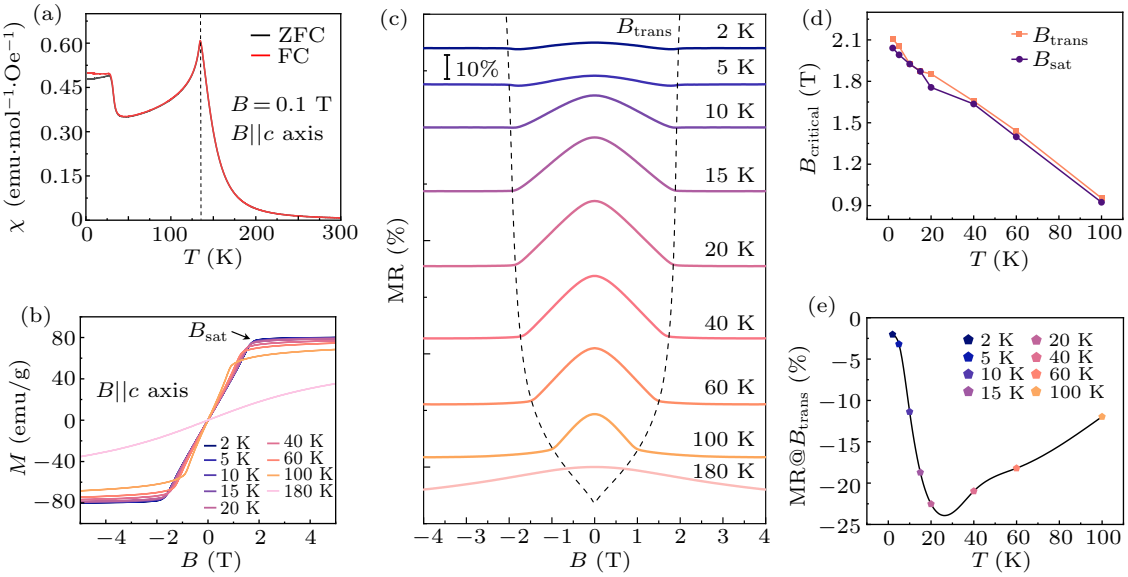


Fig. 2. Magnetic properties of CrSBr and NMR of the graphene/CrSBr heterojunction. (a) Temperature-dependent magnetization of the CrSBr bulk crystal measured under an out-of-plane external magnetic field of 0.1 T. (b) Field-dependent magnetization of CrSBr at varying temperatures under out-of-plane magnetic field. (c) Magnetoresistance ratio under out-of-plane magnetic fields from −4 T to 4 T at different temperatures. The black dashed line represents the characteristic transition field, denoted as B_{trans}. (d) Comparison between the saturation field B_{sat} (purple) and the transition field B_{trans} (orange). (e) Temperature dependence of the NMR magnitude evaluated at B_{trans}.

Several well-known mechanisms can give rise to NMR in low-dimensional systems, such as the Kondo effect, weak localization (WL), and magnetic scattering.[29–32] The NMR induced by the Kondo effect typically follows a quadratic field dependence MR $\propto B^2$, which is not observed in our device. Thus, the Kondo effect can be ruled out. In the case of WL in 2D materials, the conductivity is expected to exhibit a logarithmic temperature dependence, $\sigma_{xx} \propto \ln T$, which is also absent in the present measurements.

To quantify the correlation between the magnetic ordering of CrSBr and the transport response of the heterojunction, we extracted two characteristic fields, B_{sat} and B_{trans}, as a function of temperature (Fig. 2(d)). The two data sets nearly coincide at each temperature and exhibit essentially identical temperature dependence. This quantitative agreement indicates that the magnetoresistance (MR) response of the heterojunction is governed by the magnetic ordering of the CrSBr nanoflake. Below T_N, CrSBr develops antiferromagnetic order that becomes stronger upon cooling. Through MPE, an exchange field is induced in the adjacent monolayer graphene, leading to the spin polarization of its charge carriers. This spin polarization enhances the spin-dependent scattering. While the external magnetic field aligns the magnetic moments in CrSBr, spin-disorder scattering is progressively suppressed, resulting in the observed negative magnetoresistance (NMR). Once B exceeds B_{trans}, the CrSBr spins become nearly fully polarized, the exchange field in graphene reaches its maximum, and the spin-related scattering channel becomes field-independent, giving rise to the plateau observed in the magnetoresistance.

Figure 2(e) displays the magnitude of the maximum NMR signal evaluated at B_{trans} as a function of temperature. The

NMR magnitude does not follow a simple monotonic trend; instead, it displays a pronounced valley between 20 K and 40 K, where the curve evolves from a weak temperature dependence at higher temperatures to a steep increase upon further cooling. Similar low-temperature weak ferromagnetic signals have been reported in several independent investigations of CrSBr and have been attributed to magnetic defects (e.g., Cr vacancies, stacking faults, or canting of the antiferromagnetic sublattices) that generate uncompensated moments within an antiferromagnetic host.[28] The sudden increase of the NMR signal therefore likely reflects the combined effect of the enhanced magnetic order in the pristine lattice and the emergence of defect-related magnetic moments that further modulate the spin-dependent scattering in the monolayer graphene.

To further investigate the influence of the CrSBr layer on the charge transport in graphene, we examined the Hall response of the heterojunction below T_N. Figure 3(a) shows the Hall resistivity ρ_{xy} as a function of the out-of-plane magnetic field at various temperatures. For magnetic fields exceeding 2.1 T, ρ_{xy} exhibits a negative linear dependence, as evidenced by the ordinary Hall effect (OHE) with an electron-type charge carrier. From the linear high-field Hall response, we extracted the carrier density n_e and mobility μ using a single-band model. As shown in Fig. 3(b), the carrier density remains nearly constant with increasing temperature, while the mobility increases significantly.

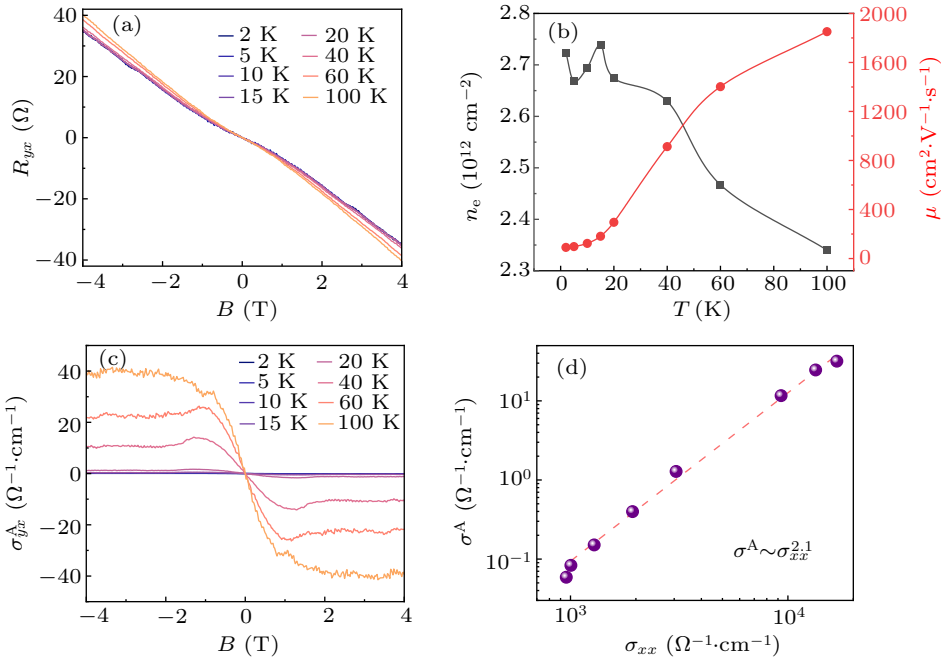


Fig. 3. Anomalous Hall effect in the graphene/CrSBr heterojunction. (a) Hall resistivity R_{yx} as a function of out-of-plane magnetic field measured at various temperatures. (b) Carrier density n_e and mobility μ extracted from the high-field linear Hall response using a single-band model. (c) Temperature dependence of the anomalous Hall conductivity σ^A_{xy}. (d) Double-logarithmic plot of σ^A_{xy} versus longitudinal conductivity σ_{xx}.

In the low-field region ($|B| < 2.1$ T), a distinct deviation from linearity is observed. This nonlinearity cannot be explained by a two-band conduction model and is therefore attributed to the AHE in graphene induced by the magnetic proximity effect. After subtracting the linear OHE background, we extracted the anomalous Hall conductivity at each temperature. As shown in Fig. 3(c), the magnitude of the anomalous Hall conductivity increases monotonically with temperature, suggesting a close connection between the AHE and carrier scattering processes. To elucidate the underlying mechanism, we plotted σ^A against σ_{xx} on a double-logarithmic scale (Fig. 3(d)). The data follow a clear power-law scaling, with a linear fit yielding a slope of 2.1, i.e., $\sigma^A \propto \sigma_{xx}^{2.1}$. This quadratic scaling, combined with the moderate σ_{xx} values (10^3–10^4 $\Omega^{-1}\cdot$ cm^{-1}), firmly places the system in the side-jump regime, particularly in the presence of magnetic disorder or strong spin–orbit coupling. Therefore, we attribute the observed AHE primarily to a side-jump scattering mechanism associated with the magnetic proximity effect induced by CrSBr.

SdH effects are observed in the graphene/CrSBr heterojunction when the magnetic field exceeds 5 T. Figure 4(a) displays the temperature dependence of the magnetoresistance ratio under magnetic fields ranging from 0 to 9 T. The pure oscillatory component ΔR_{xx} is extracted by subtracting a polynomial background (Fig. 4(b)). As shown in Fig. 4(c), the fast Fourier transform (FFT) spectra reveal two frequencies at $F_\alpha = 90$ T and $F_\beta = 171$ T. According to the Onsager relation $F = (\hbar/2\pi e)A_F$, these frequencies correspond to the extremal cross-sectional area (A_F) of the Fermi pockets perpendicular to the magnetic field. The corresponding areas are determined to be 0.00857Å^{-2} and 0.0163 Å^{-2} for F_α and F_β, respectively.

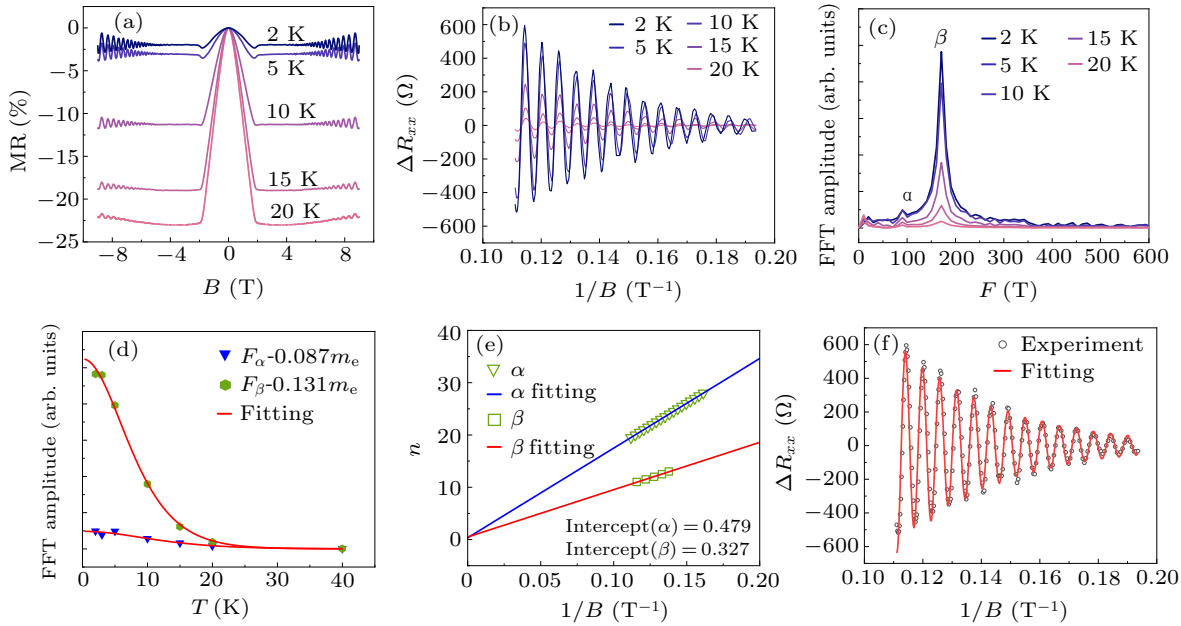


Fig. 4. SdH oscillations of the graphene/CrSBr heterojunction. (a) Magnetoresistance under out-of-plane magnetic fields from −9 T to 9 T at different temperatures. (b) The oscillatory component ΔR_{xx} as a function of $1/B$ at various temperatures. (c) Corresponding FFT amplitude, showing the α and β frequencies. (d) Temperature dependence of the FFT amplitude of F_α (blue triangles) and F_β (green dots), fitted using LK formula to extract the effective masses. (e) Landau fan diagram and the corresponding intercepts. (f) Comparison between the experimentally extracted oscillatory component of the magnetoresistance (circles) and the theoretical simulation based on the Lifshitz–Kosevich (LK) formula (solid line).

Table 1. The derived parameters from SdH oscillations for the graphene/CrSBr heterojunction.

	F (T)	K_F (Å^{-1})	A_F (nm^{-2})	m^* (m_e)	T_D (K)	τ_q (s)	μ_q (cm^2·V^{-1}·s^{-1})
α	90	0.522	0.00857	$0.087m_e$	42.33	2.872×10^{-14}	5.81×10^{2}
β	171	0.718	0.0163	$0.131m_e$	14.5	8.384×10^{-14}	1.13×10^{3}

The effective mass can be extracted by fitting the temperature dependence of the oscillation amplitude using the thermal damping term R_T in the Lifshitz–Kosevich (LK) formula, $\Delta R_{xx} \propto \frac{5}{2}\sqrt{\frac{B}{2F}} R_T R_D R_S \cos[2\pi(F/B+\gamma-\delta)]$, where $R_T = (\lambda m^* T/B)/\sinh(\lambda m^* T/B)$, $R_D = \exp(-\lambda m^* T_D/\mu_0 H)$, $R_S = \cos(\pi m^* g^*)$.[33,34] Here, m^* is the cyclotron mass, T_D is the Dingle temperature, g^* is the effective g-factor, and the constant $\lambda = 2\pi^2 k_B m_e/e\hbar \approx 14.69$ T/K. The extracted effective masses corresponding to the two frequencies are shown in Fig. 4(d). Both values are remarkably small, consistent with the characteristic of Dirac fermions in graphene. The extracted parameters for the two Fermi pockets are summarized in Table 1.

We observed that the quantum mobility extracted from SdH oscillations is significantly larger than the Hall mobility in the present system. This substantial discrepancy can be understood by considering the multiband nature of charge transport. The Hall mobility derived from a single-band model reflects a weighted average of the densities and mobilities of all carriers. In our case, the two small Fermi pockets resolved by SdH oscillations exhibit higher quantum mobility. However, due to their low carrier density, their contribution to the overall conductivity is negligible. Meanwhile, a high-density, low-mobility carrier likely exists that dominates the Hall response but remains undetected in the SdH oscillations.

Consequently, the Hall mobility is suppressed by these low-mobility carriers, while the SdH oscillations selectively probe the clean, high-mobility pockets, yielding a larger quantum mobility. Such a scenario is well-documented in other multiband systems, confirming that the observed discrepancy is physically consistent.[35,36]

The phase factor γ–δ from the LK formula is directly related to the Berry phase, where δ equals 0 for the 2D system and $\pm1/8$ for the 3D system.[37,38] Determining the Berry phase thereby provides insights into the topology of the electronic bands. Accordingly, we plotted the Landau fan diagram, as shown in Fig. 4(e). The two oscillations corresponding to different frequencies can be separated by applying a band-pass filter. The Landau indices (n) are assigned to the maxima of R_{xx} because the oscillations remain in the low-field limit.[39] According to the Lifshitz–Onsager relationship $n = \frac{F}{B} + \gamma - \delta$, the slope of the linear fit between n and $1/B$ yields the oscillatory frequency, while the intercept provides the Berry-phase information. As shown in Fig. 4(e), the intercepts for F_α and F_β are determined to be 0.479 and 0.327, respectively, indicating a 2D Fermi surface for the α pocket and a 3D Fermi surface for the β pocket. The two intercepts correspond to Berry phases of approximately -0.04π and -0.1π, both close to 0, indicating a trivial band topology. Figure 4(f) shows a two-frequency LK fit for the SdH signals, where the excellent

agreement with the experimental data confirms the reliability of the extracted parameters.

The observation of two distinct SdH frequencies provides direct evidence for the Fermi surface reconstruction in monolayer graphene induced by the adjacent CrSBr layer. These phenomena result from the collective contribution of the MPE and charge transfer at the interface. Through MPE, the exchange from CrSBr splits the Dirac cone of graphene into two spin-polarized sub-bands, breaking time-reversal symmetry and lifting the spin degeneracy. Simultaneously, charge transfer from the CrSBr layer leads to n-type doping in the monolayer graphene, shifting the Fermi level above the Dirac point. The combined effects of exchange splitting and charge transfer result in multiple Fermi pockets, giving rise to the two observed SdH oscillations. Recent first-principles calculations have confirmed this band structure reconstruction at the monolayer graphene/CrSBr interface, revealing both the exchange-induced spin splitting and charge transfer effects.[38,39] This rigid band shift caused by charge transfer is also consistent with the nearly temperature-independent n-type carrier density derived from the single-band Hall analysis. The agreement between Hall transport and quantum oscillation results thus provides strong evidence for proximity-induced spin polarization and Fermi surface reconstruction in the graphene/CrSBr heterojunction.

4. Conclusion

In conclusion, we report a magnetotransport study of high-quality graphene/CrSBr heterojunctions, demonstrating efficient spin injection and band-structure engineering in graphene via the magnetic proximity effect. The devices exhibit a pronounced NMR reaching -23% and a clear AHE below the Néel temperature of CrSBr. Magnetotransport measurements further reveal SdH oscillations with two distinct frequencies, providing direct evidence for Fermi surface reconstruction in graphene. Our results demonstrate that antiferromagnetic CrSBr can induce substantial exchange splitting and Fermi surface reconstruction in adjacent graphene, establishing the graphene/CrSBr heterojunction as a promising platform for spintronic devices.

Acknowledgements

The work is supported by the National Key Research and Development Program of China (Grant No. 2022YFA1204100), the National Natural Science Foundation of China (Grant Nos. 62488201 and 52572188), the Innovation Program of Quantum Science and Technology (Grant No. 2021ZD0302700), and the China Postdoctoral Science Foundation (Grant No. E5BK081).

References

[1] Drögeler M, Franzen C, Volmer F, Pohlmann T, Banszerus L, Wolter M, Watanabe K, Taniguchi T, Stampfer C and Beschoten B 2016 *Nano Lett.* **16** 3533
[2] Banszerus L, Schmitz M, Engels S, Dauber J, Oellers M, Haupt F, Watanabe K, Taniguchi T, Beschoten B and Stampfer C 2015 *Sci. Adv.* **1** e1500222
[3] Zatko V, Galceran R, Galbiati M, Peiro J, Godel F, Kern L M, Perconte D, Ibrahim F, Hallal A, Chshiev M, Martinez B, Frontera C, Balcells L, Kidambi P R, Robertson J, Hofmann S, Collin S, Petroff F, Martin M B, Dlubak B and Seneor P 2023 *Nano Lett.* **23** 34
[4] Tang C, Zhang Z, Lai S, Tan Q and Gao W 2020 *Adv. Mater.* **32** 1908498
[5] Asshoff P U, Sambricio J L, Rooney A P, Slizovskiy S, Mishchenko A, Rakowski A M, Hill E W, Geim A K, Haigh S J, Fal'ko V I, Vera-Marun I J and Grigorieva I V 2017 *2D Mater.* **4** 031004
[6] Lee J and Fabian J 2016 *Phys. Rev. B* **94** 195401
[7] Yang H X, Hallal A, Terrade D, Waintal X, Roche S and Chshiev M 2013 *Phys. Rev. Lett.* **110** 046603
[8] Leutenantsmeyer J C, Kaverzin A A, Wojtaszek M and Van Wees B J 2016 *2D Mater.* **4** 014001
[9] Wei P, Lee S, Lemaitre F, Pinel L, Cutaia D, Cha W, Katmis F, Zhu Y, Heiman D, Hone J, Moodera J S and Chen C T 2016 *Nat. Mater.* **15** 711
[10] Wu Y, Yin G, Pan L, Grutter A J, Pan Q, Lee A, Gilbert D A, Borchers J A, Ratcliff W, Li A, Han X and Wang K L 2020 *Nat. Electron.* **3** 604
[11] Jungwirth T, Marti X, Wadley P and Wunderlich J 2016 *Nat. Nanotechnol* **11** 231
[12] Zhou B, Balgley J, Lampen-Kelley P, Yan J Q, Mandrus D G and Henriksen E A 2019 *Phys. Rev. B* **100** 165426
[13] Marti X, Fina I and Jungwirth T 2015 *IEEE Trans. Magn.* **51** 2900104
[14] Marti X, Fina I, Frontera C, Liu J, Wadley P, He Q, Paull R J, Clarkson J D, Kudrnovský J, Turek I, Kuneš J, Yi D, Chu J H, Nelson C T, You L, Arenholz E, Salahuddin S, Fontcuberta J, Jungwirth T and Ramesh R 2014 *Nat. Mater.* **13** 367
[15] Moriyama T, Matsuzaki N, Kim K J, Suzuki I, Taniyama T and Ono T 2015 *Appl. Phys. Lett.* **107** 122403
[16] Che B, Hu G, Zhu C, Guo H, Lv S, Liu X, Wu K, Zhao Z, Pan L, Zhu K, Qi Q, Han Y, Lin X, Li Z A, Shen C, Bao L, Liu Z, Zhou J, Yang H and Gao H J 2024 *Chin Phys. B* **33** 027502
[17] Qiao Z, Ren W, Chen H, Bellaiche L, Zhang Z, MacDonald A H and Niu Q 2014 *Phys. Rev. Lett.* **112** 116404
[18] Ziebel M E, Feuer M L, Cox J, Zhu X, Dean C R and Roy X 2024 *Nano Lett.* **24** 4319
[19] Klein J and Ross F M 2024 *J. Mater. Res.* **39** 3045
[20] Guo J, Shi W, Ni K, Chen X, Liu D, Liu X, Wang S, Li Q, Xiao R C and Yang M 2025 *Chin Phys. B* **34** 104203
[21] Shcherbakov D, Stepanov P, Weber D, Wang Y, Hu J, Zhu Y, Watanabe K, Taniguchi T, Mao Z, Windl W, Goldberger J, Bockrath M and Lau C N 2018 *Nano Lett.* **18** 4214
[22] Yang B, Bhujel B, Chica D G, Telford E J, Roy X, Ibrahim F, Chshiev M, Cosset-Chéneau M and Wees B J V 2024 *Nat. Commun.* **15** 4459
[23] Scheie A, Ziebel M, Chica D G, Bae Y J, Wang X, Kolesnikov A I, Zhu X and Roy X 2022 *Adv. Sci.* **9** 2202467
[24] Beck J 1990 *Z. Anorg. Allg. Chem.* **585** 157
[25] PPizzocchero F, Gammelgaard L, Jessen B S, Caridad J M, Wang L, Hone J, Bøggild P and Booth T J 2016 *Nat. Commun.* **7** 11894
[26] Ye C, Wang C, Wu Q, Liu S, Zhou J, Wang G, Söll A, Sofer Z, Yue M, Liu X, Tian M, Xiong Q, Ji W and Renshaw Wang X 2022 *ACS Nano* **16** 11876
[27] Telford E J, Dismukes A H, Lee K, Cheng M, Wieteska A, Bartholomew A K, Chen Y, Xu X, Pasupathy A N, Zhu X, Dean C R and Roy X 2020 *Adv. Mater.* **32** 2003240
[28] Telford E J, Dismukes A H, Dudley R L, Wiscons R A, Lee K, Chica D G, Ziebel M E, Han M G, Yu J, Shabani S, Scheie A, Watanabe K, Taniguchi T, Xiao D, Zhu Y, Pasupathy A N, Nuckolls C, Zhu X, Dean C R and Roy X 2022 *Nat. Mater.* **21** 754
[29] Wang X, Yang Y, Li Y, Liu G, Duan J, Wang Z, Lu L and Yang F 2025 *Phys. Rev. B* **112** 165204
[30] Li C Z, Wang L X, Liu H, Wang J, Liao Z M and Yu D P 2015 *Nat. Commun.* **6** 10137

[31] Karki Chhetri S, Acharya G, Graf D, Basnet R, Rahman S, Sharma M M, Upreti D, Nabi M R U, Kryvyi S, Sakon J, Mortazavi M, Da B, Churchill H and Hu J 2025 *Phys. Rev. B* **111** 014431

[32] Liu H, Xue Y, Shi J A, Guzman R A, Zhang P, Zhou Z, He Y, Bian C, Wu L, Ma R, Chen J, Yan J, Yang H, Shen C M, Zhou W, Bao L and Gao H J 2019 *Nano Lett.* **19** 8572

[33] Qi Q, Lv S, Zhu K, Xie Y, Hu G, Zhao Z, Xian G, Han Y, Yang Y, Bao L, Lin X, Guo H, Yang H and Gao H J 2025 *Chin Phys. B* **34** 077305

[34] Fu Y, Zhao N, Chen Z, Yin Q, Tu Z, Gong C, Xi C, Zhu X, Sun Y, Liu K and Lei H 2021 *Phys. Rev. Lett.* **127** 207002

[35] Ding L, Koo J, Yi C, Xu L, Zuo H, Yang M, Shi Y, Yan B, Behnia K and Zhu Z 2021 *J. Phys. D: Appl. Phys.* **54** 454003

[36] Liang T, Gibson Q, Ali M N, Liu M, Cava R J and Ong N P 2015 *Nat. Mater.* **14** 280

[37] Mikitik G P and Sharlai Yu V 1999 *Phys. Rev. Lett.* **82** 2147

[38] Luk'yanchuk I A and Kopelevich Y 2004 *Phys. Rev. Lett.* **93** 166402

[39] Xiang F X, Wang X L, Veldhorst M, Dou S X and Fuhrer M S 2015 *Phys. Rev. B* **92** 035123

[40] Rassekh M and Gmitra M 2026 *Phys. Rev. B* **113** 035126

[41] Mao R, Feng Z and Li Z 2026 *Appl. Surf. Sci.* **732** 166508